Alkane Functionalization at Nonheme Iron Centers. Stoichiometric Transfer of Metal-Bound Ligands to Alkane

Takahiko Kojima, Randolph A. Leising, Shiping Yan, and Lawrence Que, Jr.*

Contribution from the Department of Chemistry, University of Minnesota, Minneapolis, Minnesota 55455

Received May 24, 1993[®]

Abstract: A series of $[Fe^{III}X_2L]^+$ complexes (L = TPA, tris(2-pyridylmethyl)amine, or NTB*, tris(N-ethylbenzimidazol-2-ylmethyl)amine; X = Br, Cl, or N_3) has been synthesized and examined for their ability to activate alkyl hydroperoxides for the functionalization of alkanes at room temperature. The crystal structures of $[FeCl_2(TPA)]ClO_4$ (**2**) and $[Fe_2-OCl_2(TPA)_2](ClO_4)_2$ (**6**) were determined, while other complexes were characterized by their visible and NMR spectra. Treatment of the mononuclear complexes with a stoichiometric amount of alkyl hydroperoxide in the presence of cyclohexane affords halocyclohexane in good yield. The production of bromo- and azidocyclohexane was correlated with the disappearance of the characteristic LMCT bands of the mononuclear catalysts, which were converted into catalytically inactive (μ-oxo)diferric species. The yield of haloalkane increased to 100% based on complex when an excess of alkyl hydroperoxide was used, but it was not affected by the addition of excess halide. The formation of haloalkane was inhibited by the presence of dimethyl sulfide (forming DMSO), but was unaffected by the addition of 4-methyl-2,6-di-*tert*-butylphenol, suggesting the involvement of a two-electron oxidant in the reaction mechanism. The selectivities of the catalysts for cyclohexane and adamantane functionalization were significantly affected by the nature of the tripodal ligand and the bound halide but not by the alkyl group on the hydroperoxide. We thus propose the active species to be $[O{=}Fe(L)(X)]^{2+}$, which may be related to the transient intermediate generated from the reaction of $Fe_2O(TPA)_2(ClO_4)_4$ with H_2O_2 (Leising et al. *J. Am. Chem. Soc.* **1991**, *113*, 3988–3990). In the proposed mechanism, $[O{=}Fe(L)(X)]^{2+}$ abstracts hydrogen from the alkane and then transfers the bound halide to the incipient alkyl radical. Such an oxidative ligand transfer reaction has been proposed for the mechanism of thiazolidine ring formation in penicillin biosynthesis by the nonheme iron enzyme isopenicillin N synthase.

Introduction

The functionalization of saturated hydrocarbons under mild conditions has been of great interest because the abundance of alkanes in nature makes them convenient industrial and chemical feedstocks.[1] Industrial efforts to utilize alkanes as starting materials require energy-intensive conditions because of their inertness toward chemical conversion.[2] In sharp contrast, nature has evolved a number of enzymes to perform such conversions selectively and under very mild conditions.[3]

Among biological catalysts, cytochromes P-450 activate dioxygen to hydroxylate saturated hydrocarbons and epoxidize olefins via the formation of a putative (porphyrin[•+])$Fe^{IV}{=}O$ species; such a species is reminiscent of compound I in the catalytic cycle of horseradish peroxidase.[4] Moreover, the addition of peroxides to the ferric enzyme allows the same reactions to be performed via a peroxide shunt pathway.[5]

Nonheme iron enzymes, on the other hand, are just beginning to be characterized.[3] Methane monooxygenase (MMO)[6] has a diiron active site which catalyzes the hydroxylation of alkanes including methane.[7] Fatty acyl desaturase has recently been demonstrated to have a related diiron site[8] and presumably functions by hydroxylating the alkyl chain following by dehydration. α-Ketoglutarate-dependent enzymes have mononuclear

iron active sites which hydroxylate unactivated C–H bonds in proline, lysine, aspartate, and thymine concomitant with the oxidative decarboxylation of the keto acid.[9] Mononuclear nonheme iron enzymes are involved in the biosynthesis of isopenicillin N, cephalosporin C, and clavaminate;[9b,10] in these reactions an unactivated C–H bond is transformed into a C–X bond (X = O, S), where the heteroatom is part of the substrate molecule. In studies on isopenicillin N synthase (IPNS), Baldwin has proposed that the thiazolidine ring forms by oxidative ligand transfer (OLT) as shown in Figure 1. In these reactions the active species has been proposed to be a high-valent iron–oxo species by analogy to the heme enzymes; but detailed reaction mechanisms have yet to be established.

There have been several efforts aimed at modeling the alkane functionalization chemistry of nonheme iron enzymes;[11] most prominent of these are the catalysts collectively known as the

[®] Abstract published in *Advance ACS Abstracts*, November 1, 1993.

(1) Sheldon, R. A; Kochi, J. K. *Metal-Catalyzed Oxidations of Organic Compounds*; Academic: New York, 1981.

(2) Mimoun, H. In *Comprehensive Coordination Chemistry*; Wilkinson, G, Gillard, R. D.; McCleverty, J. A., Eds.; Pergamon Press: Oxford, 1987; Vol. 6.

(3) Que, L., Jr. in *Bioinorganic Catalysis*; Reedijk, J., Ed.; Marcel Dekker: New York, 1993; pp347–393.

(4) Ortiz de Montellano, P. R. In *Cytochrome P-450: Structure, Mechanism, and Biochemistry*; Ortiz de Montellano, P. R., Ed.; Plenum: New York, 1986; Chapter 7.

(5) McMurry, T. J.; Groves, J. T. In *Cytochrome P-450: Structure, Mechanism, and Biochemistry*; Ortiz de Montellano, P. R., Ed.; Plenum: New York, 1986; Chapter 1.
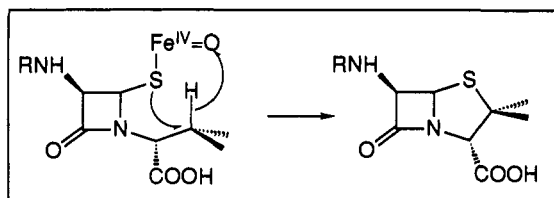
(6) Abbreviations used: BHT, 4-methyl-2,6-di-*tert*-butylphenol; BPA, bis-(2-pyridylmethyl)amine; bpy, 2,2′-bipyridyl; CHP, cumene hydroperoxide; CyBr, bromocyclohexane; CyCl, chlorocyclohexane; CyN$_3$, azidocyclohexane; CyOH, cyclohexanol; CyO, cyclohexanone; CyOO'Bu, *tert*-butyl cyclohexyl peroxide; DBC, 3,5-di-*tert*-butylcatecholate dianion; DPPH, 2,2-diphenyl-1-picrylhydrazyl; IPNS, isopenicillin N synthase; KIE, kinetic isotope effect; MMO, methane monooxygenase; NTB, tris(benzimidazol-2-ylmethyl)amine; NTB*, tris((N-ethylbenzimidazol-2-yl)methyl)amine; OLT, oxidative ligand transfer; TBHP, *tert*-butyl hydroperoxide; TPA, tris(2-pyridylmethyl)amine; TPP, 5,10,15,20-tetraphenylporphine dianion.

(7) (a) DeWitt, J. G.; Bentsen, J. G.; Rosenzweig, A. C.; Hedman, B.; Green, J.; Pilkington, S.; Papaefthymiou, G. C.; Dalton, H.; Hodgson, K. O.; Lippard, S. J. *J. Am. Chem. Soc.* **1991**, *113*, 9129–9135. (b) Fox, B. G.; Froland, W. A.; Dege, J. E.; Lipscomb, J. D. *J. Biol. Chem.* **1989**, *264*, 10023–10033. (c) Froland, W. A.; Andersson, K. K.; Lee, S.-K.; Liu, Y.; Lipscomb, J. D. *J. Biol. Chem.* **1992**, *267*, 17588–17597. (d) Andersson, K. K.; Froland, W. A.; Lee, S.-K.; Lipscomb, J. D. *New J. Chem.* **1991**, *15*, 411–415.

(8) Fox, B. G.; Shanklin, J.; Somerville, C.; Münck, E. *Proc. Natl. Acad. Sci. U.S.A.* **1993**, *90*, 2486–2490.

(9) (a) Udenfriend, S.; Cardinale, G. In *Oxygenases and Oxygen Metabolism*; Nozaki, M., Ed.; Academic: New York, 1982; pp 99–110. (b) Townsend, C. A.; Basak, A. *Tetrahedron* **1991**, *47*, 2591–2602.

(10) (a) Robinson, J. A. *Chem. Soc. Rev.* **1988**, *17*, 383–452. (b) Baldwin, J. E.; Abraham, E. *Nat. Prod. Rep.* **1988**, *5*, 129–145.

Figure 1. Proposed mechanism for thiazolidine ring formation by IPNS.

"Gif" system.[12] A major drawback in understanding the inorganic chemistry of the "Gif" catalysts is the difficulty in defining the metal coordination environment. In order to alleviate this problem, we have used tetradentate tripodal ligands to fix four of the coordination sites of the metal center. The ligand TPA (tris(2-pyridylmethyl)amine) in particular has been a versatile and effective ligand in these investigations. We have found that mononuclear and oxo-bridged dinuclear Fe(TPA) complexes are efficient catalysts for the alkyl hydroperoxide-dependent hydroxylation of cyclohexane.[13] In the course of these studies, we have discovered that the mononuclear [FeX$_2$(TPA)]$^+$ complexes effect stoichiometric functionalization of cyclohexane by oxidative ligand transfer (OLT) forming halocyclohexanes.[14] We detail our mechanistic insights in this paper.

Experimental Section

Materials. All chemicals were of reagent grade unless otherwise noted. Acetonitrile (HPLC grade/glass distilled) was purchased from Fisher Scientific or EM Science and used as received. Methanol was obtained from EM Science and dried over alumina. *tert*-Butyl hydroperoxide (70% in H$_2$O), cumene hydroperoxide (80% in H$_2$O), and adamantane were purchased from Aldrich. Cyclohexane and Na$_2$SO$_4$ were obtained from Fisher. Azidocyclohexane was synthesized by the nucleophilic substitution of cyclohexyl tosylate by NaN$_3$.[15] 1- and 2-chloroadamantanes were synthesized by the substitution of corresponding alcohols by SOCl$_2$.[16] 1-Azidoadamantane was synthesized as reported by Sasaki et al.[17] 2-Azidoadamantane was synthesized from the reaction of 2-aminoadamantane and *n*-butyl lithium in THF followed by *p*-tosyl azide; the desired azide was purified by silica gel column chromatography by elution with hexanes.[18] The tripodal ligands, TPA·3HClO$_4$[19] and *N*-Et-NTB (NTB*)[20] were synthesized by following published procedures. **Caution:** The perchlorate salts and azide derivatives are all potentially explosive and should be handled with care.[21]

Synthesis. [FeBr$_2$(TPA)](ClO$_4$) (1) A solution containing 0.59 g of TPA·3HClO$_4$ (1.0 mmol) and 0.10 g (1.0 mmol) of triethylamine in 50 mL of methanol was warmed (to ~60 °C) to dissolve all of the ligand. To this solution was added 0.30 g of Fe^{III}Br$_3$ (1.0 mmol) dissolved in 2 mL of methanol. The solution was allowed to cool to room temperature

overnight during which time red crystals formed (76% yield). Anal. Calcd for C$_{18}$H$_{18}$Br$_2$ClFeN$_4$O$_4$: C, 35.71; H, 3.00; N, 9.25. Found: C, 36.04; H, 3.28; N, 9.30.

[FeCl$_2$(TPA)](ClO$_4$) (2) was synthesized using the procedure outlined for **1** replacing FeBr$_3$ with FeCl$_3$·6H$_2$O, resulting in the formation of long yellow crystals (50% yield). Anal. Calcd for C$_{18}$H$_{18}$Cl$_3$FeN$_4$O$_4$: C, 41.85; H, 3.51; N, 10.85. Found: C, 42.06; H, 3.80; N, 10.56.

[Fe(N$_3$)$_2$(TPA)]ClO$_4$ (3). To a solution of acid-free TPA (0.145 g, 0.5 mmol) in 30 mL of methanol under Ar were added Fe(ClO$_4$)$_3$·10H$_2$O (0.267 g, 0.5 mmol) and NaN$_3$ (81 mg, 1.25 mmol). The mixture was stirred for 5 h with warming, and the volume was reduced under vaccum. Filtration afforded a thick red powder. Isolated yield, 70%. Anal. Calcd for C$_{18}$H$_{18}$ClFeN$_{10}$O$_4$: C, 40.81; H, 3.43; N, 26.44. Found: C, 40.80; H, 3.60; N, 26.39.

[FeCl$_2$(NTB*)]Cl (4). To a solution of NTB* (0.98 g, 2 mmol) in 40 mL of methanol was added FeCl$_3$·4H$_2$O (0.47 g, 2 mmol) in 10 mL of methanol under air. The mixture was stirred for 1 h. A red-orange powder was obtained in 94% yield. Anal. Calcd for C$_{30}$H$_{33}$Cl$_3$FeN$_7$: C, 55.11; H, 5.09; N, 15.00; Cl, 16.27. Found: C, 54.98; H, 5.16; N, 14.74; Cl, 16.57.

[FeBr$_2$(NTB*)]Br (5). To a solution of NTB* (0.20 g, 0.41 mmol) and 15 equiv of HBr (48%) in 30 mL of methanol under Ar was added FeBr$_3$ (0.120 g, 0.41 mmol) in 3 mL of methanol. The solution was stirred for 2 h and the volume was reduced under vacuum to obtain a red powder in 82% yield. Anal. Calcd for C$_{30}$H$_{33}$Br$_3$FeN$_7$: C, 45.77; H, 4.23; N, 12.46. Found: C, 45.86; H, 4.36; N, 12.34.

[Fe$_2$OCl$_2$(TPA)$_2$](ClO$_4$)$_2$ (6) was synthesized by addition of 0.531 g of FeCl$_3$·6H$_2$O (1.0 mmol) in 2 mL of methanol to a solution of 0.591 g of TPA·3HClO$_4$ (1.0 mmol) and 6.3 mL (4.5 mmol) of triethylamine in 40 mL of methanol. The solution was allowed to stand for 2 h during which time yellow-brown crystals formed and then 0.268 g of crystalline material was isolated (50% yield). Anal. Calcd for [Fe$_2$OCl$_2$(TPA)$_2$]-(ClO$_4$)$_2$, C$_{37}$H$_{37}$Cl$_3$Fe$_2$N$_8$O$_{15}$: C, 42.25; H, 3.54; N, 10.65. Found: C, 42.06; H, 3.80; N, 10.56.

[Fe$_2$OBr$_2$(TPA)$_2$](ClO$_4$)$_2$ (7) was synthesized by addition of 0.150 g of FeBr$_3$ (0.51 mmol) in 2 mL of methanol to a solution of 0.30 g of TPA·3HClO$_4$ (0.51 mmol) and 0.23 g (2.3 mmol) of triethylamine in 20 mL of methanol. The solution was allowed to stand for 2 h during which time a yellow-brown powder formed in 95% yield. Anal. Calcd for [Fe$_2$-OBr$_2$(TPA)$_2$](ClO$_4$)$_2$, C$_{37}$H$_{37}$Br$_2$Cl$_2$Fe$_2$N$_8$O$_{15}$: C, 40.52; H, 3.40; N, 10.50. Found: C, 40.67; H, 3.37; N, 10.29.

Instrumentation. Visible spectra were recorded on a Hewlett-Packard 8541A diode array spectrometer. Product analyses were carried out on Perkin-Elmer Sigma 3 and AutoSystem Gas chromatographs with flame-ionization detection using an Alltech HELIFLEX AT-1701 (30 m × 0.25 mm o.d.; film thickness, 0.25 μm) column for cyclohexane derivatives and an Alltech AT-WAX (15 m × 0.54 mm o.d.; film thickness, 1.2 μm) column for the adamantane products. ^{1}H-NMR spectra and T_1 values were measured on IBM AC 300 and Varian VXR 300 spectrometers at 300 MHz. Chemical shifts for Fe(III) complexes (in ppm) were referenced to the residual protic solvent peak. Cyclic voltammetry was conducted by a BIOANALYTICAL Systems model CV-1A-120 instrument using a Pt working electrode at 25 °C under Ar with 0.1 M [(n-Bu)$_4$N]BF$_4$ as an electrolyte in acetonitrile. The redox potentials (mV) were determined versus SCE by using ferrocene as a reference.

Oxidative Ligand Transfer Reactions (OLT). The OLT reactions to cyclohexane and cyclohexene were conducted by using 3.0 mM complex and 1.15 M substrate with various amounts of alkyl hydroperoxides (ROOH) in acetonitrile at room temperature under Ar. For OLT reactions to adamantane, 15 mM adamantane was reacted with 3.0 mM complex and 3.0 mM ROOH in acetonitrile–benzene (1:1 v/v) at room temperature under Ar. The reaction mixture was quenched with the same volume of aqueous 0.4 M Na$_2$SO$_4$ solution, followed by extraction with 3 × 2 mL of diethyl ether. The ether layer was collected and dried over anhydrous Na$_2$SO$_4$. Toluene (for both cyclohexane and cyclohexene reactions) or *o*-dichlorobenzene (for the adamantane reaction) was added at this point as an internal standard, and the mixture was analyzed by GC. Retention times and yields of products were confirmed by injections of authentic compounds.

Catalytic Oxygenation. In a typical reaction, 0.77 M cyclohexane was reacted with 0.10 M TBHP in the presence of 0.7 mM complex in acetonitrile at room temperature under Ar. For adamantane oxygenation, 0.21 M adamantane was reacted with 70 mM TBHP in the presence of 0.7 mM complex in acetonitrile–benzene (1:1 v/v). Workup was conducted as in the OLT reactions.

(11) (a) Groves, J. T.; Van Der Puy, M. *J. Am. Chem. Soc.* **1976**, *98*, 5290–5297. (b) Sugimoto, H.; Sawyer, D. T. *J. Am. Chem. Soc.* **1985**, *107*, 5712–5716. (c) Kitajima, N.; Fukui, H.; Moro-oka, Y. *J. Chem. Soc., Chem. Commun.* **1988**, 485. (e) Fish, R. H.; Konings, M. S.; Oberhausen, K. J.; Fong, R. H.; Yu, W. M.; Christou, G.; Vincent, J. B.; Coggin, D. K.; Buchanan, R. M. *Inorg. Chem.* **1991**, *30*, 3002–3006. (f) Tung, H.-C.; Kang, C.; Sawyer, D. T. *J. Am. Chem. Soc.* **1992**, *114*, 3445–3455.

(12) Barton, D. H. R.; Doller, D. *Acc. Chem. Res.* **1992**, *25*, 504–512 and references cited therein.

(13) (a) Leising, R. A.; Norman, R. E.; Que, L., Jr. *Inorg. Chem.* **1990**, *29*, 2553–2555. (b) Leising, R. A.; Kim, J.; Pérez, M. A.; Que, L., Jr. *J. Am. Chem. Soc.* **1993**, *115*, 9524–9530.

(14) Leising, R. A.; Zang, Y.; Que, L., Jr. *J. Am. Chem. Soc.* **1991**, *113*, 8555–8557.

(15) *Vogel's Textbook of Practical Organic Chemistry*, 5th ed.; Furniss, B. S., Hannaford, A. J., Smith, P. W. G., Tatchell, A. R., Eds.; Longman Scientific & Technical: England, 1989; p 886.

(16) Reference 15, p 558.

(17) Sasaki, T.; Eguchi, S.; Katada, T.; Hiroaki, O. *J. Org. Chem.* **1977**, *42*, 3741–3743.

(18) (a) Doering, W. von E.; DePuy, C. H. *J. Am. Chem. Soc.* **1953**, *75*, 5955–5957. (b) Steinheimer, T. R.; Wulfman, D. S.; McCullagh, L. N. *Synthesis* **1971**, 325–326. (c) Sasaki, T.; Eguchi, S.; Toi, N. *Heterocycles* **1977**, *7*, 315–320.

(19) (a) Gafford, B. G.; Holwerda, R. A. *Inorg. Chem.* **1989**, *28*, 60–66. (b) Anderegg, G.; Wenk, F. *Helv. Chim. Acta* **1967**, *50*, 2330–2332.

(20) Hendriks, H. M. J.; Birker, P. J. M. W.; Verschoor, G. C.; Reedijk, J. *J. Chem. Soc., Dalton Trans.* **1982**, 623–631.

(21) (a) Wolsey, W. C. *J. Chem. Educ.* **1973**, *50*, A335–A337. (b) Raymond, K. N. *Chem. Eng. News* **1983**, *61*, (Dec. 5), 4.

Table I. Crystallographic Data and Computation[a] for [FeCl₂(TPA)]₂[Fe₂OCl₂(TPA)₂](ClO₄)₄ (2 and 6)

empirical formula	$C_{72}H_{72}Cl_{10}Fe_4N_{16}O_{17}$
formula wt	2011.39
cryst size, mm³	0.04 × 0.20 × 0.30
temp, °C	−90
space group	$P2_1/c$ (No. 14)
a, Å	13.772(9)
b, Å	12.671(6)
c, Å	23.621(11)
β, deg	91.53(4)
V, Å³	4121(7)
Z	2
D_{calc}, g cm⁻³	1.621
radiation	Mo Kα λ = 0.71069 Å)
μ, cm⁻¹	6.64
scan method	ω
$2\theta_{max}$, deg	48
indices collected	+h, +k, ±l
no. of reflctns measd	6640
reflctns used ($I > 1.0\sigma(I)$)	3660
no. of variables used	449
R, R_w[b]	0.065, 0.055

[a] The intensity data were processed as described in: *CAD 4 and SDP-PLUS User's Manual*; B.A. Frenz & Assoc.; College Station, TX, 1982. The net intensity $I = [K(NPI)](C - 2B)$, where $K = 20.1166$ (attenuator factor), NPI = ratio of fastest possible scan rate to scan rate for the measurement, C = total count, and B = total background count. The standard deviation in the net intensity is given by $[\sigma(I)]^2 = (k/NPI)^2[C + 4B + (pI)^2]$ where p is a factor used to downweight intense reflections. The observed structure factor amplitude F_o is given by $F_o = (I/LP)^{1/2}$, where LP = Lorentz and polarization factors. The $\sigma(I)$'s were converted to the estimated errors in the relative structure factors $\sigma(F_o)$ by $\sigma(F_o) = 1/2[\sigma(I)/I]F_o$. [b] $R = \Sigma||F_o| - |F_c||/\Sigma|F_o|$; $R_w = [(\Sigma w(|F_o| - |F_c|)^2/\Sigma wF_o^2)]^{1/2}$.
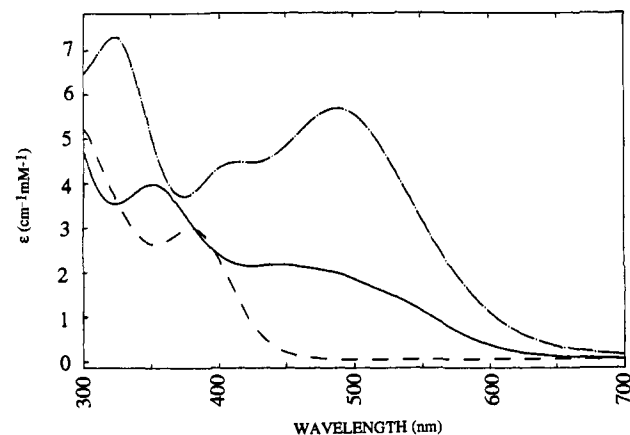
Figure 2. UV–vis spectra of [FeX₂(TPA)]⁺ complexes in acetonitrile: **1** (—); **2** (−−); **3** (·−·).

X-ray crystallography of 2 and 6. Complexes **2** and **6** co-crystallized from methanol solution, permitting the elucidation of the structures of both complexes with a single crystal. The crystal was mounted on a glass fiber and coated with viscous hydrocarbon. Data were collected on an Enraf-Nonius CAD4 diffractometer using graphite-monochromated Mo Kα (λ = 0.72069 Å) radiation and the ω-scan method. Three standard reflections were measured every 100 min and showed negligible decay. Empirical absorption and Lorentz–polarization absorption corrections were made. The crystallographic data are collected in Table I.

The structure was solved by direct methods. All calculations were performed by using the TEXSAN crystallographic software package of the Molecular Structure Corp. All non-hydrogen atoms were refined with anisotropic thermal parameters. Hydrogen atoms were included in the structure correlation in idealized positions (d(C–H) = 0.95 Å, B_{iso} = 3.0) and not refined anisotropically. Refinement was carried out by using full-matrix least-squares techniques with scattering factors[22] and anomalous dispersion terms.[23] The final difference Fourier map showed no significant residual peak and the largest peak was found with 0.681

(22) Cromer, D. T. *International Tables for X-ray Crystallography*; Kynoth Press: Birmingham, England; Vol. IV, Table 2.2 A.

Table II. ¹H NMR Chemical Shifts and Absorption Maxima for [FeX₂(TPA)]⁺ (1–3) and [Fe₂OX₂(TPA)₂]²⁺ (6, 7) Complexes

compd	chemical shifts, ppm	λ_{max}, nm (ϵ, M⁻¹ cm⁻¹)
1 (X = Br)	249, 198 (pyr α, br), 170 (C*H*₂) 144, 114, 113, 98 (pyr β, β')	350 (4400) 454 (2380)
2 (X = Cl)	245 (pyr α, br), 165 {0.1}[c] (C*H*₂), 137 {0.9},[c] 112 {0.9},[c] 98 {1.0}[c] (pyr β, β')	382 (3170)
3 (X = N₃)	206 (pyr α, br), 135 (C*H*₂) 118, 103 (pyr β, β')	494 (5240) 408 (sh)
6 (X = Cl)	33, 29 (pyr α), 20 (C*H*₂), 17.7, 16.7, 12.9, 11.5 (pyr β, β'), 7.5, 7.1 (pyr γ)	380 (8300)
7 (X = Br)	34, 29 (pyr α), 21 (C*H*₂), 17.9, 16.7 12.6, 11.1 (pyr β, β'), 7.4, 6.7 (pyr γ)	400 (sh) (4350) 492 (sh) (720)

[a] Measured in CD₃CN, residual solvent peak as a reference. [b] Measured in CH₃CN. [c] Braces indicate T_1 (ms).
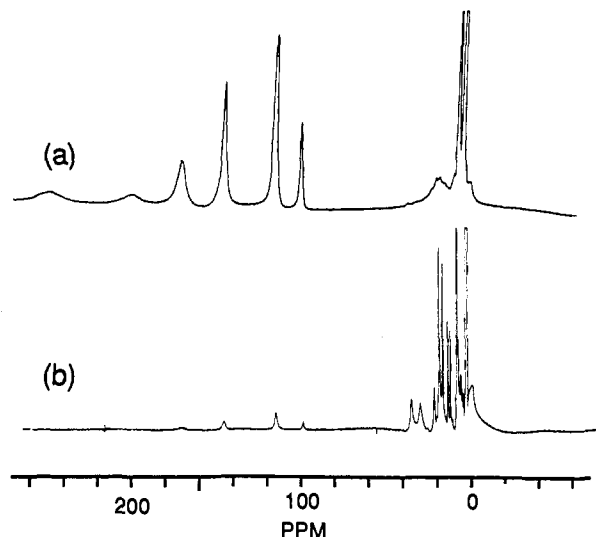
Figure 3. ¹H NMR spectra of **1** and cyclohexane-d_{12} in CD₃CN at room temperature under Ar: (a) before the addition of TBHP; (b) 30 min after the addition of TBHP (see text).

e/Å³ near a ClO₄⁻. Final atomic coordinates and anisotropic thermal factors of **2** and **6** can be found in the supplementary material.

Results

Synthesis and Characterization of Complexes. A series of mononuclear [FeX₂(L)]⁺ (X = Br, Cl, N₃; L = TPA, NTB*) complexes has been synthesized to investigate ligand effects on the oxidative ligand transfer reaction to cyclohexane. The complexes were readily obtained from reaction mixtures in moderate yield. However, [FeBr₂(NTB*)]Br and [Fe(N₃)₂-(TPA)]ClO₄ were prone to hydrolysis, forming μ-oxo dimer species, and greater care must be taken to minimize the amount of trace water in the reaction mixture. The introduction of the ethyl group on the benzimidazole ring nitrogen in NTB* resulted in a significantly higher solubility of the complexes relative to that of the NTB complexes, thus facilitating our study.

The UV–vis spectra of **1–3** in CH₃CN are shown in Figure 2 and absorption properties are listed in Table II. For **1**, an absorption band ascribed to the charge transfer transition from Br⁻ to Fe^III can be observed at 454 nm (ϵ = 2380 M⁻¹ cm⁻¹). For **2**, the absorption maximum shifts to 382 nm (ϵ = 3170 M⁻¹ cm⁻¹), consistent with the LMCT assignment. For **3**, absorption features are observed at 408 (sh) and 494 nm (ϵ = 5240 M⁻¹ cm⁻¹) and assigned to azide-to-Fe(III) LMCT transitions. **6**, the μ-oxo derivative of **2**, has absorption bands at 315 (sh) and 380 nm (ϵ = 820 M⁻¹ cm⁻¹), while **7**, the μ-oxo derivative of **1**, has features at 340 (sh) and 498 nm (ϵ = 720 M⁻¹ cm⁻¹). **2** and **6** have similar

(23) Cromer, D. T. *International Tables for X-ray Crystallography*; Kynoth Press: Birmingham, England; Vol. IV, Table 2.3.1.
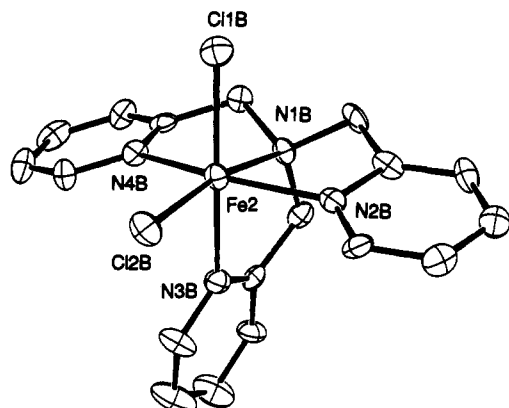
Figure 4. ORTEP representation of the cation {FeCl₂(TPA)]⁺ (2) thermal ellipsoids. Hydrogen atoms have been omitted for clarity.

absorption maxima; however, **7** is readily distinguished from **1** by UV–vis spectroscopy.

The ¹H NMR spectra of **1–5** in CD₃CN exhibit large paramagnetic shifts when compared with those of μ-oxo complexes because of the absence of strong antiferromagnetic coupling.[24] The spectrum of **1** is shown in Figure 3a; NMR assignments for all complexes are listed in Table II. The spectra of **1–3** consist of broad features similar to those observed for [Fe(DBC)(TPA)]-BPh₄.[6,25] The β and β′ protons of the TPA pyridine rings appear as three peaks near 100 ppm in a 2:3:1 intensity pattern. As seen in the structure of **2**, two of the pyridine rings are trans to each other and one pyridine ring is trans to a halide ligand; thus a 2:2:1:1 pattern of peaks is expected for the pyridine β and β′ protons, consistent with the observed spectrum. The methylene protons are assigned to the broad peak at 170 ppm, while the pyridine α protons are assigned to broad bands near 250 and 200 ppm. The pyridine γ protons are lost within the large solvent peak in the diamagnetic region.
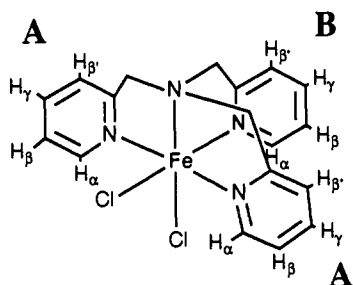
Cyclic voltammetry (CV) performed on **1–5** in acetonitrile at 25 °C shows reversible redox waves for all complexes. In the TPA series, $E_{1/2}$ (vs. SCE) values are 144 mV for **1**, –14 mV for **2**, and –201 mV for **3**. In the NTB* series, corresponding values are 166 mV for **4** and –60 mV for **5**. The trends observed within each ligand series reflect the expected order in the X ligand basicities.

Molecular Structures of [FeCl₂(TPA)]ClO₄ (2) and [Fe₂OCl₂-(TPA)₂](ClO₄)₂ (6). Crystals of a 2:1 mixture of **2** and **6** were obtained from methanol solution. The complexes co-crystallized in the space group $P2_1/c$ (No. 14), and the crystallographic data are summarized in Table I.

The ORTEP representation of the [FeCl₂(TPA)]⁺ cation is shown in Figure 4, and selected bond lengths and angles are listed in Table III. Complex **2** has a distorted octahedral geometry, as represented by the trans ligand angles of 153.3(3)° for ∠N2B–Fe₂–N4B, 169.3(2)° for ∠Cl1B–Fe₂–N1B, and 169.1(2)° for

(24) Norman, R. E.; Holz, R. C.; Ménage, S.; O'Connor, C. J.; Zhang, J. H.; Que, L., Jr. *Inorg. Chem.* **1990**, *29*, 4629–4637.

(25) Jang, H. G.; Cox, D. D.; Que, L., Jr. *J. Am. Chem. Soc.* **1991**, *113*, 9200–9204.

Table III. Selected Bond Lengths (Å) and Angles (deg) for [FeCl₂(TPA)](ClO₄) (2) and [Fe₂OCl₂(TPA)₂](ClO₄)₂ (6)[a]

[FeCl₂(TPA)](ClO₄) (2)			
Fe2–Cl1B	2.267(3)	Fe2–Cl2B	2.224(2)
Fe2–N1B	2.202(6)	Fe2–N2B	2.119(7)
Fe2–N3B	2.199(7)	Fe2–N4B	2.133(7)
Cl1B–Fe2–Cl2B	97.81(9)	Cl1B–Fe2–N1B	92.6(2)
Cl1B–Fe2–N2B	95.0(2)	Cl1B–Fe2–N3B	169.1(2)
Cl1B–Fe2–N4B	91.6(2)	Cl2B–Fe2–N1B	169.3(2)
Cl2B–Fe2–N2B	100.2(2)	Cl2B–Fe2–N3B	91.7(2)
Cl2B–Fe2–N4B	104.5(2)	N1B–Fe2–N2B	76.2(3)
N1B–Fe2–N3B	78.2(3)	N1B–Fe2–N4B	77.7(3)
N2B–Fe2–N3B	88.5(3)	N2B–Fe2–N4B	153.3(3)
N3B–Fe2–N4B	80.8(3)		
[Fe₂OCl₂(TPA)₂](ClO₄)₂ (6)			
Fe1–O11	1.790(1)	Fe1–Cl1	2.319(2)
Fe1–N1A	2.202(6)	Fe1–N2A	2.127(7)
Fe1–N3A	2.263(6)	Fe1–N4A	2.114(6)
Fe1⋯Fe1	3.581(2)		
Fe1–O11–Fe1	179.98(0)	Cl1–Fe1–O11	101.22(7)
Cl1–Fe1–N1A	165.7(2)	Cl1–Fe1–N2A	102.6(2)
Cl1–Fe1–N3A	89.0(2)	Cl1–Fe1–N4A	101.6(2)
O11–Fe1–N1A	93.1(2)	O11–Fe1–N2A	88.6(2)
O11–Fe1–N3A	167.8(2)	O11–Fe1–N4A	94.3(2)
N1A–Fe1–N2A	77.5(2)	N1A–Fe1–N3A	76.8(2)
N1A–Fe1–N4A	77.1(2)	N2A–Fe1–N3A	82.5(2)
N2A–Fe1–N4A	154.5(2)	N3A–Fe1–N4A	90.1(2)

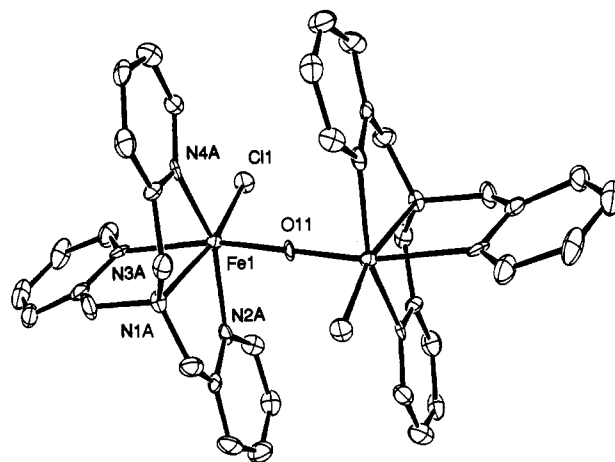[a] For atom labels, see Figure 4 for **2** and Figure 5 for **6**, respectively.

Figure 5. ORTEP drawing of the cation [Fe₂OCl₂(TPA)₂]²⁺ (6) showing 50% thermal ellipsoids. Hydrogen atoms have been omitted for clarity.

∠Cl1B–Fe2–N3B. Moreover, the angle for ∠Cl1B–Fe–Cl2B is 97.81(9)°, which is significantly larger than 90°. As is often the case with a tripodal ligand that forms 5-membered chelate rings, the coordination geometry is distorted toward the tertiary amino group (average ∠N_{amine}–Fe–N_{pyridine} = 77.4°). The Fe–N(pyridine) bonds (av 2.17 Å) are shorter than the Fe–N(amine) bond (2.202(6) Å), in the range of other Fe(III)–TPA complexes already reported.[25,26] Consequently the Fe2–Cl2B bond which is trans to the tertiary amino group (2.244(2) Å) is shorter than the Fe2–Cl1B bond trans to a pyridyl moiety (2.267(3) Å).

The crystal structure of the [Fe₂OCl₂(TPA)₂]²⁺ cation is presented in Figure 5. This μ-oxo dimer **6** has a linear Fe–O–Fe structure as required by the center of symmetry at the bridging oxygen. The Fe–μ-O bond distance is 1.790(1) Å, which is within the range of reported (μ-oxo)diiron(III)–TPA complexes.[24,26] Fe–N_{py} (av 2.17 Å) and Fe–N_{amine} (2.202(6) Å) distances are also typical for those complexes. The chloride ligands coordinate trans

(26) (a) Yan, S.; Cox, D. D.; Pearce, L. L.; Juarez-Garcia, C.; Que, L., Jr.; Zhang, J. H.; O'Connor, C. J. *Inorg. Chem.* **1989**, *28*, 2507–2509. (b) Norman, R. E.; Yan, S.; Que, L., Jr.; Backes, G.; Ling, J.; Sanders-Loehr, J.; Zhang, J. H.; O'Connor, C. J. *J. Am. Chem. Soc.* **1990**, *112*, 1554–1562.

11332 *J. Am. Chem. Soc., Vol. 115, No. 24, 1993*

Kojima et al.

Table IV. Product Distributions for the Iron-Catalyzed TBHP Oxidation of Cyclohexane in Acetonitrile under Ar at Room Temperature

compd	eq TBHP[a]	rxn time, h	products[b] CyX	other products
1 (X = Br)	1	1	0.8	
1 under CO	1	1	0.8	
1[c]	150	0.5	1	9 (CyOH) 13 (CyO) 9 (CyOO^{t}Bu)
1/1000 eq [(n-Bu)$_4$N]Br	150	0.5	1	
1/15 mM BHT	5	0.5	1	
1/100 eq Me$_2$S	1	1	0	1 (DMSO)
2 (X = Cl)	1	1	0.7	
3 (X = N$_3$)	1	4	0.8	
4 (X = Br)	1	24	0.5	
5 (X = Cl)	1	24	0.3	
[FeBr$_3$(BPA)][d]	20	20	2	1 (CyOH) 1 (CyO) 3 (CyOO^{t}Bu)

[a] Relative to catalyst. [b] Amount = moles of product/moles of catalyst. [c] Reference 13a. [d] Reference 14.

Figure 6. Time course of bromocyclohexane production and visible absorption change at 500 nm in the reaction of 1 with TBHP and cyclohexane at –25 °C under Ar.

to the amine nitrogen on each iron center and *anti* to each other relative to the Fe–O–Fe axis. The Fe–Cl bond lengths are comparable to those of [Fe$_2$O(OAc)$_2$Cl$_2$(bpy)$_2$].[27]

Oxidative Ligand Transfer Reactions. We have recently found that [FeX$_2$TPA]ClO$_4$ complexes, together with *tert*-butyl hydroperoxide, are efficient reagents for the stoichiometric functionalization of cyclohexane.[14] These results are summarized in Table IV. A 1:1 combination of complex and ROOH affords 70–80% yield of cyclohexyl halide based on oxidant. This reaction is thus among the most efficient in utilizing oxidizing equivalents to functionalize alkanes. On the other hand, the (μ-oxo)diferric complexes 6 and 7 were ineffective in carrying out the reaction. When the tripodal ligand TPA is replaced with NTB*, the yields decrease by approximately 50% and the reaction times increase by an order of magnitude (Table IV). The fact that alkyl halide is the only product of the reaction facilitates our mechanistic investigation.

A number of experiments were conducted to gain insight into the mechanism of the reaction. The time courses of the reactions of 1 and 3 with TBHP were followed by UV–vis spectroscopy concurrently with the formation of CyBr and CyN$_3$ by GC. In the case of 1, the reaction was followed at –25 °C to slow the reaction sufficiently to allow convenient sampling. The yield of CyBr and the absorbance change at 500 nm as a function of time are shown in Figure 6. From the graphs, it is clear that the absorption at 454 nm disappears concomitant with the formation of CyBr. In the case of 3, the formation of CyN$_3$ was also coincident with the disappearance of absorption features at 408 and 494 nm in the UV–vis spectrum. These results suggest a role for the metal center in the reaction.

The change in the complex during the reaction can also be monitored by NMR. The ^{1}H NMR spectrum of the mixture of 1 and cyclohexane-d_{12} in CD$_3$CN showed large paramagnetic shifts (Figure 3a) as expected for the mononuclear complex. Thirty minutes after the addition of 1 equiv of TBHP, the spectrum changed to that of an antiferromagnetically coupled (μ-oxo)-diferric complex, [Fe$_2$OBr$_2$(TPA)$_2$]$^{2+}$ (7) (Figure 3b), which was independently synthesized and presumably has a structure similar to that of 6. Similar spectral changes could be observed for the 2/TBHP/cyclohexane-d_{12} system. Thus the mononuclear complex is converted to a μ-oxo dimer upon the consumption of TBHP.

Increasing the amount of TBHP added served to increase the yield of alkyl halide formed but only to the stoichiometric
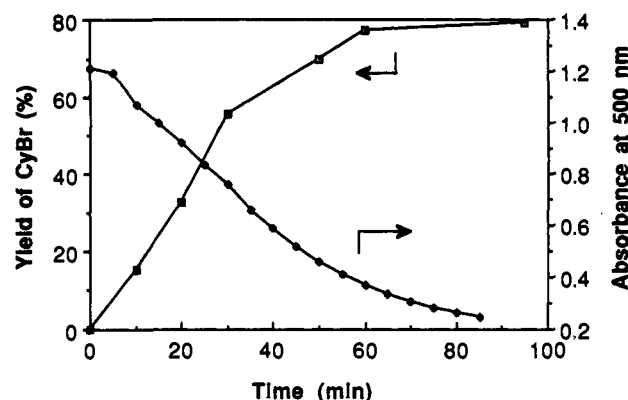
maximum of one per metal complex. The remaining oxidizing equivalents gave rise to oxygenated products such as cyclohexanol, cyclohexanone, and *tert*-butyldioxycyclohexane.[13] The maximum yield of alkyl halide was unaffected by added halide (up to 1000-fold excess); however, the added halide decreased the yield of oxygenated products. Indeed when 1000-fold halide was added, only the 1 equiv of alkyl halide was formed and most of the TBHP added remained unreacted. These observations suggest that free halide is not incorporated into the alkane and the reagent responsible for halogenation differs from that responsible for oxygenation.

When Fe(BPA)Br$_3$ was used as catalyst, a maximum of 2 equiv of alkyl bromide was observed.[14] This complex has three coordinated bromide ligands, compared to the two in 1. The doubling of the bromoalkane yield in the case of the BPA catalyst suggests that one halide dissociates from the metal center to promote the OLT and the halides remaining on the metal center are transferred onto the alkane.

Reagents designed to trap reactive intermediates were added to provide further insight. Replacing the Ar atmosphere with CO did not affect the yield of alkyl halide formed. This result is distinct from that observed by Barton *et al.*[28] and suggests that alkyliron species are unlikely to be involved, as proposed for Gif-type chemistry.[12] The addition of 4-methyl-2,6-di-*tert*-butylphenol did not affect the yield of CyX, but 100 equiv of Me$_2$S completely inhibited formation of CyX; indeed 1 equiv of DMSO was formed instead. 4-Methyl-2,6-di-*tert*-butylphenol is a one-electron reductant, while Me$_2$S traps 2e$^-$ oxidants. These observations implicate the participation of a 2e$^-$ oxidant in the reaction.

Kinetic isotope effects (KIE), k_H/k_D, for the various complexes were determined by using a 1:1 mixture of cyclohexane–cyclohexane-d_{12} (Table V). The results show that a primary KIE can be observed for each system, indicating that hydrogen abstraction from substrate is an important step in the reaction mechanism. The KIEs for the TPA complexes monotonically increased from 7 to 8 to 9 for the bromide (1), chloride (2), and azide (3) complexes, respectively. In the case of the NTB* complexes, the KIE for the bromide complex (4) was 10, while that for the chloride complex (5) could not be determined because of the very low yield of CyCl-d_{11}. These observations show that the nature of L and X affects the oxidizing power of the reagent.

The selectivity of the reagents for abstracting the tertiary and secondary hydrogens of adamantane was determined to further assess the relative reactivity of the active species (Table V). For our study, the 3°/2° ratio is defined as [3° product]/[2° product] multiplied by 3, the latter factor to compensate for the larger number of secondary H's on adamantane. Note that the selectivity

(27) Vincent, J. B.; Huffman, J. C.; Christou, G.; Li, Q.; Nanny, M. A.; Hendrickson, D. N.; Fong, R. H.; Fish, R. H. *J. Am. Chem. Soc.* **1988**, *110*, 6898–6900.

(28) Barton, D. H. R.; Csuhai, E.; Doller, D. *Tetrahedron Lett.* **1992**, *33*, 4389–4392.

Table V. Comparison of the Reactivities of the Various Complexes toward Cyclohexane and Adamantane under Stoichiometric OLT and Catalytic Hydroxylation Conditions

com-plexes	rxn time, h	cyclo-hexane k_H/k_D	adamantane selectivity $(3°/2°)^a$			
			R–X[b] (TBHP)	R–X[b] (CHP)	R–OH[c] (TBHP)	R–OH[c] (CHP)
1	1	7	5	6	7	7
2	1	8	10	9	7	7
3	4	9	10	11	7	6
4	20	10	8	n.d.[d]	n.d.[d]	n.d.[d]
5	20		13	n.d.[d]	n.d.[d]	n.d.[d]

[a] $3°/2°$ ratio $= 3 \times [3°$ product]$/[2°$ product]. [b] Under stoichiometric OLT conditions. [c] Under catalytic hydroxylation conditions. [d] Not determined.

of the reagent increases when bromide is replaced by chloride and when TPA is replaced by NTB*, but substituting CHP for TBHP has little or no effect. Those observations indicate that the nature of L and X in $[FeX_2(L)]^+$ affects the selectivity of the active species with respect to hydrogen abstration from the substrate, but the alkyl substituent on ROOH does not. In contrast, the selectivity for the catalytic hydroxylation of adamantane with excess ROOH and $[FeX_2(TPA)]^+$ was independent of X and R, suggesting that the oxidant responsible for the halogenation reaction differs from that responsible for hydroxylation and that all starting mononuclear complexes are converted to the same hydroxylating agent.

When the 2/TBHP/adamantane reaction was conducted in the presence of 10% CH_2Br_2, both bromoadamantanes and chloroadamantanes were observed as products. The $3°/2°$ ratio for each compound was determined to be 5 for chloroadamanatanes and 14 for bromoadamantanes, values which differ significantly from those obtained in the absence of CH_2Br_2. Scrutiny of the amounts of products formed showed that the yield of 2-chloroadamantane (2°) decreased only slightly relative to the reaction in the absence of CH_2Br_2, while the amount of 1-chloroadamantane (3°) dropped significantly. The decreases in the amounts of chloroadamanatanes corresponded to the amounts of bromoadamantanes formed, indicating that CH_2Br_2 intercepted some of the alkyl intermediate formed and diverted it toward bromoalkane products. Indeed the combined $3°/2°$ ratio for adamantyl halides was calculated to be 9.5, a value almost identical to that observed for the 2/TBHP/adamantane reaction in the absence of CH_2Br_2.

Lastly, the functionalization of cyclohexene was examined. The reaction of cyclohexene with 1/TBHP or 2/TBHP gave only allylic products in nearly stoichiometric yield and no epoxide. Both the 3-halocyclohexene and cyclohex-2-en-1-ol were observed, but the latter was found to derive from the hydrolysis of the 3-halocyclohexene products. These observations indicate a strong preference of the active species to abstract hydrogen from an allylic C–H group rather than to epoxidize olefins.

Discussion

The stoichiometric functionalization of cyclohexane by $[FeX_2-(TPA)]^+/ROOH$ provides a unique opportunity to examine the mechanism of alkane C–H bond cleavage by a nonheme iron catalyst. The observations presented in the Results section can be rationalized by the mechanism shown in Figure 7. The reaction is initiated by a ligand exchange reaction wherein a ligand halide is replaced by alkyl peroxide presumably via a dissociative pathway. Heterolysis of the peroxide O–O bond then affords a high-valent iron–oxo species which abstracts hydrogen from alkane and then transfers the X ligand to the nascent alkyl radical to form the C–X bond. The fact that the halogenation reaction is unaffected by the addition of 4-methyl-2,6-di-*tert*-butylphenol excludes the possibility that peroxide homolysis occurs to generate alkoxy radicals which then abstract hydrogen from substrate. Furthermore, alkyl halide cannot derive from alkyl radicals that
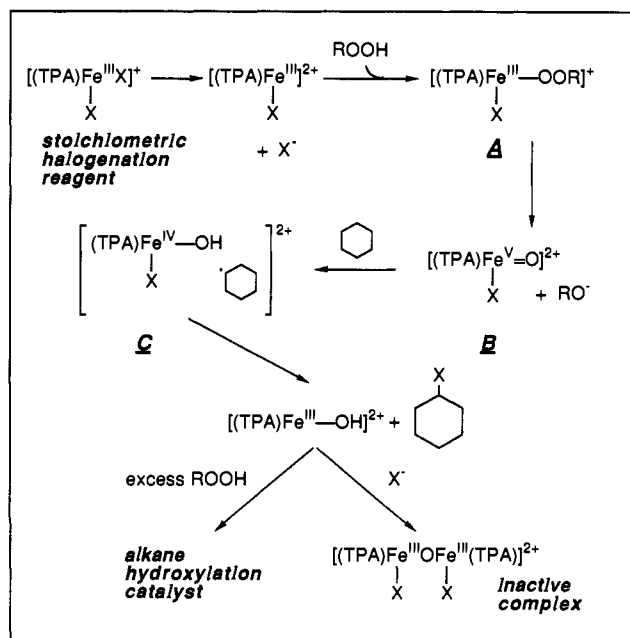

Figure 7. Proposed reaction mechanism for the oxidative ligand transfer reaction.

are free in solution to react with starting complex. Such a mechanism has been ascribed to the alkane functionalization reactions of Mn(TPP)X in concert with iodosylbenzene which are inhibited by the radical scavenger DPPH.[29] On the other hand, Me_2S completely inhibits the halogenation reaction. While inhibition by Me_2S may result from its binding to the five-coordinate $[LFeX]^{2+}$ in competition with ROOH, it is unlikely that the oxophilic high-spin ferric center would favor binding to the soft Me_2S over the harder alkyl hydroperoxide. Furthermore the production of 1 equiv of DMSO in place of RX argues for the interception of a 2e⁻ oxidant formed in the course of the reaction,[30] which may be either the Fe^{III}—OOR complex (species A) or the Fe=O species (species B) in Figure 7.

Evidence that the metal center is the halogenating agent comes from the following observations: (a) that the maximum yield of alkyl halide is stoichiometric with $[FeLX_2]^+$ reagent, (b) that excess halide does not increase the yield of alkyl halide, and (c) that $Fe(BPA)Br_3$, a complex with three coordinated bromides, affords a maximum of 2 equiv of alkyl halide per catalyst molecule. Thus one halide must dissociate from the starting complex to provide a site for ROO⁻ binding and the remaining halides in the metal coordination sphere may be oxidatively transferred to the substrate. These reactions are therefore best described as oxidative ligand transfer (OLT) reactions.

The nature of the reactive species is further indicated by the cyclohexane kinetic isotope effects and the adamantane selectivity data (Table V). The fact that the selectivity of substrate halogenation depends on L and X suggests that the oxidizing power of the reactive species is modulated by the electronic properties of L and X. This means that the species responsible for hydrogen abstraction must be formulated to include L and X. The choices are thus narrowed down to intermediate A or B in Figure 7. The observation that the alkyl group on ROOH does not significantly affect the selectivity leads us to favor species B. In any case, species B must be derived from species A via O–O bond heterolysis. Peroxide O–O bond homolysis of species A to form an alkoxy radical that abstracts hydrogen from substrates can be excluded because substrate selectivity should then be independent of metal complex, which would be inconsistent with our observations.

(29) Smegal, J. A.; Hill, C. L. *J. Am. Chem. Soc.* **1983**, *105*, 3515–3521.
(30) Labeque, R.; Marnett, L. J. *J. Am. Chem. Soc.* **1989**, *111*, 6621–6627.

The notion of a high-valent iron–oxo species is presently accepted for the active species in cytochrome P450-catalyzed hydroxylations.[4,31] An analogous species in a nonheme environment has been proposed as the intermediate generated from the reaction of $[Fe_2O(TPA)_2](ClO_4)_4$ with H_2O_2.[32] Although no such intermediate can directly be observed in the OLT reactions, we can infer its participation and some details of its structure from a comparison of the reactivities of the different OLT reagents.

In the next step of the mechanism, we propose that species B reacts with substrate and abstracts hydrogen from a C–H bond, engendering species C. Species C is formulated as a radical cage by analogy to corresponding species in heme-catalyzed alkane hydroxylations.[33] The cage is proposed for the OLT reaction to rationalize the high efficiency of ligand transfer per ROOH, the lack of alkyl radical coupling byproducts, and the failure of 4-methyl-2,6-di-*tert*-butylphenol to affect the reaction. The nascent alkyl radical would appear to be trapped by X very soon after its formation.

The collapse of the cage to form R–X is where the OLT mechanism differs from that of heme-catalyzed hydroxylation. Groves has introduced the notion of oxygen rebound to describe the C–O bond forming step in the mechanism.[33] In species C of the OLT mechanism, the radical has two potential pathways for decomposition, by oxygen rebound to form alcohol or by halide transfer to form R–X. It is clear from our results that halide transfer is overwhelmingly favored over oxygen rebound. This conclusion is easily rationalized when one compares the redox potential of OH⁻ versus those of the halides. In other words, if the functionalization of R is viewed simplistically as the coupling of R• and X•, the halide radicals being of lower potential (Br⁻ + e⁻ → Br⁻, 1.07 V vs SHE; Cl• + e⁻ → Cl⁻, 1.36 V; HO• + e⁻ → OH⁻, 2.02 V)[34] would be transferred more readily. This preference is also consistent with the expected oxophilicity of high-valent iron.

We also considered the possibility that electron transfer from the alkyl radical to the iron center may occur, forming an alkyl cation and an Fe(III) center in the cage. In this case, R–X formation should depend on the nucleophilicities of OH vs the halides. Since hydroxide is the most nucleophilic of the anions involved,[35] alcohol formation would be expected to prevail, contrary to our results. Therefore, we conclude that C–X bond formation proceeds via radical coupling rather than via an ionic mechanism. A similar mechanism is favored in the halogenation of alkyl radicals by Cu(II) complexes.[36]

The release of the RX leaves $[LFe^{III}-OH]^{2+}$. As shown in the mechanism in Figure 7, this species can proceed in two ways, depending on the presence of more ROOH or halide. In the presence of more ROOH, $[LFe^{III}-OH]^{2+}$ reacts with ROOH and alkane to afford the oxygenated products in the catalytic reaction. When all the ROOH is consumed, $[LFe^{III}-OH]^{2+}$ dimerizes and combines with dissociated halide to form a (μ-oxo)diferric complex $[Fe_2OL_2X_2]^{2+}$. This species is readily observed in the NMR spectrum of the reaction mixture at the end of the reaction (Figure 3). The addition of excess halide inhibits the catalytic reaction but not the OLT reaction; indeed at a 1000-fold excess of bromide, only the OLT product is observed in stoichiometric yield. In the scheme presented in Figure 7,

excess halide may bind to $[LFe-X]^{2+}$ or $[LFe-OH]^{2+}$. In the first scenario excess halide would inhibit the formation of species A, thereby shutting down both the OLT and the catalytic hydroxylation reactions, which is contrary to our observations. In the second scenario, excess halide would affect only the catalytic hydroxylation reaction by diverting the $[LFe^{III}-OH]^{2+}$ intermediate into the catalytically inactive $[Fe_2OX_2L_2]^{2+}$ complex. Our observations are thus consistent with the second scenario.

The $[LFe^{III}-OH]^{2+}$ species is the point of convergence for all OLT reactions; with no more bound halide to modulate its properties, the reaction with ROOH (R = *t*-Bu, cumyl) engenders an oxidant that has an adamantane selectivity for hydroxylation independent of the nature of the starting X anion as shown in Table V. Thus the reactive species responsible for the hydroxylation reaction differs from those involved in the OLT reactions. Further work to identify intermediates in the catalytic hydroxylation reaction is in progress.

We have thus described an oxidative ligand transfer reaction from metal center to alkane and provided arguments for the participation of a high-valent iron–oxo species in a nonheme environment (species B in Figure 7). Such species are proposed in the mechanisms of alkane functionalization catalyzed by methane monooxygenase,[8] isopenicillin N synthase,[10] and α-keto acid-dependent iron hydroxylases.[10,37] Because we have chosen to investigate a system with a well-defined coordination chemistry, our present results allow us to infer details of the coordination environment of the active species. Furthermore, the high conversion efficiency of the TBHP oxidizing equivalent into R–X also lends credence to our mechanistic conclusions.

Our results are of relevance to several aspects of the alkane functionalization field. First, the reactions reported in this paper represent the first demonstrated functionalization of alkanes by oxidative ligand transfer. While previous halogenations of alkanes under oxidizing conditions[38] may also proceed by this mechanism, the reactions were not studied in sufficient detail to allow such a conclusion to be reached. Oxidative ligand transfer has been proposed as the mechanism for forming the thiazolidine ring in the reaction catalyzed by isopenicillin N synthase (Figure 1)[10b] and for forming the furan ring in the reaction catalyzed by clavaminate synthase.[9b] These reactions are proposed to utilize an $Fe^{II}/Fe^{IV}=O$ redox couple, whereas the oxidative ligand transfer we describe uses an $Fe^{III}/Fe^{V}=O$ redox couple; nevertheless, our studies provide the first evidence that such a mechanism is viable.

Second, the mechanism we propose differs from that favored by Barton for the "Gif" family of alkane oxygenation catalysts.[12] Barton proposes the formation of an alkyliron(V)–hydroxy species derived from the [2 + 2] addition of a C–H bond to an iron-(V)–oxo moiety.[12] He has argued that the properties of the alkyl species generated in "Gif" chemistry differ significantly from those expected of free radicals. There may only be a semantic difference between an alkyliron(V) moiety and the caged radical species C in Figure 7, since the cage may introduce sufficient constraints on the behavior of the radical so as to modify its reactivity *vis-à-vis* that of a free radical. The TPA chemistry differs from the "Gif" chemistry in at least one respect. While running the OLT reaction under CO has no effect on the product of the reaction, the presence of CO results in the formation of carboxylic acid products in "Gif" chemistry.[28] It has been suggested that the appearance of such products results from the insertion of CO into an alkyliron bond affording an acyliron species.

Third, the addition of CH_2Br_2 alters the 3°/2° ratio for the OLT reaction to adamantane. The 3°/2° ratio for the 2-catalyzed OLT reaction is 9.7 in the absence of CH_2Br_2. The addition of CH_2Br_2 decreases this value to 5 for the chloroadamantane

(31) Marnett, L. J.; Weller, P.; Battista, J. R. In *Cytochrome P-450: Structure, Mechanism, and Biochemistry*; Ortiz de Montellano, P. R், Ed.; Plenum: New York, 1986; Chapter 2.

(32) Leising, R. A.; Brennan, B. A.; Que, L., Jr.; Fox, B. G.; Münck, E. *J. Am. Chem. Soc.* **1991**, *113*, 3988–3990.

(33) Groves, J. T. *J. Chem. Educ.* **1985**, *62*, 928–931.

(34) *CRC Handbook of Chemistry and Physics*; Weast, R. C., Ed.; CRC Press: Florida, 1984; p D-156.

(35) Carey, F. A.; Sundberg, R. J. *Advanced Organic Chemistry*, 3rd ed.; Plenum: New York, 1990; Part A, p 284–290.

(36) (a) Kochi, J. K. In *Frontiers of Free Radical Chemistry*; Pryor, W. A., Ed.; Academic: New York, 1980; pp 297–353. (b) Kochi, J. K. In *Free Radicals*; Kochi, J. K., Ed.; Wiley: New York, 1973; Vol. I, pp 591–683.

(37) Chiou, Y.-M.; Que, L., Jr. *J. Am. Chem. Soc.* **1992**, *114*, 7567–7568.

(38) Sugimoto, H.; Sawyer, D. T. *J. Org. Chem.* **1985**, *50*, 1784–1786.

products and results in the formation of bromoadamantanes with a 3°/2° ratio of 14. However, when all adamantyl halides are considered together, the 3°/2° ratio is 9.5, a value essentially identical to that obtained in the absence of CH_2Br_2. These observations show that the selectivity of the catalyst in abstracting hydrogen from adamantane is not altered by the addition of CH_2-Br_2. What is altered is the fate of the alkyl radical. In the context of our proposed scheme, the caged radical is presented with a choice of reacting with the metal-bound halide or the CH_2Br_2. The tertiary adamantyl radical appears to be trapped more readily by CH_2Br_2, thus affording the large 3°/2° ratio for bromoadamantanes.

A similar mechanism may explain the unusual selectivity attributed to the "Gif" catalysts for attack at secondary carbon. Ratios of 3°/2° as low as 0.5[39] have been reported in the "Gif^{IV}" system when only the oxygenated adamantane products were considered in the calculation.[40] However, subsequent studies revealed the formation of *tert*-adamantylpyridines in significant quantities,[41] demonstrating that tertiary adamantyl radicals were formed in the reaction but were trapped by the solvent pyridine. When all substituted adamantane products were considered in the calculation, the 3°/2° ratio turned out to be $\sim$3, showing that abstraction of the tertiary C–H was still favored over the secondary C–H.[42] In both "Gif" and OLT reactions tertiary adamantyl radicals appear to be more readily trapped than corresponding secondary radicals.

Last, we compare the reactivity of the iron–oxo species implicated in the OLT reaction *vis-à-vis* the analogous heme species. With respect to cyclohexene, the heme species can act as both an oxo-transfer agent and a hydrogen-atom-abstraction agent forming cyclohexene oxide and cyclohex-2-en-1-ol, respectively, but yields primarily the epoxide product.[43] The nonheme species in our system does not epoxidize cyclohexene at all but effects functionalization solely at the allylic position. This preference for hydrogen abstraction over oxo transfer by the latter represents one important reactivity difference between heme and nonheme iron–oxo species and may indicate greater radical character for the nonheme moiety. Further studies comparing the reactivity of heme versus nonheme iron species should be carried out to characterize the role of the ligands in mediating hydrocarbon oxidations.

Supplementary Material Available: Tables of atomic coordinates, bond lengths and angles, and anisotropic thermal factors of the non-hydrogen atoms of **2** and **6** (8 pages). Ordering information is given on any current masthead page.

(39) These ratios have been re-calculated to conform to our definition of the 3°/2° ratios found in Table V.

(40) Barton, D. H. R.; Boivin, J.; Gastiger, M.; Morzycki,, J.; Hay-Motherwell, R. S.; Motherwell, W. B.; Ozbalik, N.; Schwartzentruber, K. M. *J. Chem. Soc., Perkin Trans. 1* **1986**, 947–955.

(41) Barton, D. H. R.; Boivin, J.; Motherwell, W. B.; Ozbalik, N.; Schwartzentruber, K. M. *Nouv. J. Chim.* **1986**, *10*, 387–398.

(42) Barton, D. H. R.; Halley, F. Ozbalik, N.; Schmitt, M.; Young, E.; Balavoine, G. *J. Am. Chem. Soc.* **1989**, *111*, 7144–7149.

(43) (a) Groves, J. T.; Nemo, T. E. *J. Am. Chem. Soc.* **1983**, *105*, 5786–5791. (b) Traylor, T. G.; Pann, W.-P.; Bandyopadhyay, D. *J. Am. Chem. Soc.* **1989**, *111*, 8009–8010.